Improving Predictions of Stream CO_2 Concentrations and Fluxes using a Stream Network Model: a Case Study in the East River Watershed, CO, USA

Brian Saccardi[1] and Matthew Winnick[1]

[1]Department of Geoscience, University of Massachusetts, Amherst.

Corresponding author: Brian Saccardi (bsaccardi@umass.edu)

Key Points:

- We present a stream network model that accurately predicts stream $p\mathrm{CO_2}$ and fluxes through representation of physical hydrologic processes
- Inverse correlations between $p\mathrm{CO_2}$ and atmosphere exchange velocities cause up to 13x overestimates of river CO_2 fluxes from statistical upscaling
- Model-data comparisons suggest that internal CO_2 sources account for roughly half of watershed CO_2 fluxes through hyporheic zone respiration

Abstract

Rivers and streams are an important component of the global carbon budget, emitting CO_2 to the atmosphere. However, our ability to accurately predict carbon fluxes from stream systems remains uncertain due to small scales of $p$$CO_2$ variability within streams (10^0-10^2 m), which make monitoring intractable. Here we incorporate CO_2 input and output fluxes into a stream network advection-reaction model, representing the first process-based representation of stream CO_2 dynamics at watershed scales. This model includes groundwater (GW) CO_2 inputs, water column and benthic hyporheic zone (BZ) respiration, downstream advection, and atmospheric exchange. We evaluate this model against existing statistical methods including upscaling techniques and multiple linear regression models through comparisons to high-resolution stream $p$$CO_2$ data collected across the East River Watershed in the Colorado Rocky Mountains. The stream network model accurately captures topography-driven $p$$CO_2$ variability and significantly outperforms multiple linear regressions for predicting $p$$CO_2$. Further, the model provides estimates of CO_2 contributions from internal versus external sources and suggests that streams transition from GW- to BZ-dominated sources between 3rd and 4th Strahler orders, with GW and BZ accounting for 53 and 47% of CO_2 fluxes from the watershed, respectively. Lastly, stream network model CO_2 fluxes are 5-13x times smaller than upscaling technique predictions, largely due to inverse correlations between stream $p$$CO_2$ and atmosphere exchange velocities. Taken together, the stream network model presented improves our ability to predict and monitor stream CO_2 dynamics, and future applications to regional and global scales may result in a significant downward revision of global flux estimates.

Plain Language Summary

Rivers and streams are an important part of the global carbon cycle, contributing carbon dioxide to the atmosphere. However, the amount of carbon dioxide these systems contribute is notoriously difficult to measure as it changes over short spatial scales. In this paper we present a method of modeling carbon dioxide that uses the current understanding of sources, transport, and reactions that carbon dioxide undergoes in these systems. This model is compared to previous methods of predicting carbon dioxide contributions from streams, using data collected in the East River Watershed in the Colorado Rocky Mountains. We find that the process-based model presented here is more accurate than current methods of predicting carbon dioxide contributions from rivers to the atmosphere. Furthermore, the model suggests that carbon dioxide produced within the stream corridor, as opposed to soil and groundwater sources, contributed roughly half of watershed stream carbon dioxide fluxes. Finally, we show that previous methods for modeling stream carbon dioxide overestimate watershed fluxes by as much as 13x; therefore, the application of a process-based model to larger systems may result in a large decrease in global estimates of stream carbon dioxide fluxes.

1 Introduction

Inland waters have been recognized as an important component of the carbon cycle, connecting terrestrial carbon (C) to the oceans and atmosphere (Cole et al., 2007). Among inland waters, rivers and streams are the largest contributors of CO_2 accounting for 70% of total fluxes (Raymond et al., 2013). Within rivers and streams, headwater are often considered hotspots of CO_2 evasion contributing roughly 30% of the 0.7 - 3.88 Pg of C yr^{-1} inland waters emit to the atmosphere (Drake et al., 2018; Lauerwald et al., 2015; Marx et al., 2017; Raymond et al., 2013). Currently efforts to monitor and predict CO_2 fluxes depend on accurate stream pCO_2 estimates derived from pH, temperature, and alkalinity (Marx et al., 2017; Raymond et al., 2013) or using direct measurements (Sawakuchi et al., 2017). However, these types of measurements are not feasible to deploy at the scales (10^0-10^2 m) required to capture the spatial variability of pCO_2 within stream networks. Due to this inability to measure stream CO_2 with adequate resolution, global fluxes remain highly uncertain and are continuously revised using new statistical scaling models and river data products (Allen & Pavelsky, 2018; Horgby et al., 2019b; Sawakuchi et al., 2017). While the processes that control CO_2 variability and fluxes along stream networks are relatively well characterized, current flux budgets rely exclusively on empirical and statistical upscaling or modeling efforts.

Specifically, efforts to quantify large-scale stream CO_2 fluxes generally employ one of two methodologies: statistical upscaling or multiple linear regression analysis. Upscaling efforts typically use statistical distributions of pCO_2 observations, often categorized by Strahler stream order, and apply these to unmeasured regions (Butman & Raymond, 2011; Raymond et al., 2013). Alternatively, a number of studies have used statistical regressions to predict pCO_2 based on readily available environmental variables such as elevation, soil organic carbon content, discharge (Q), and areal wetland extent (Borges et al., 2015; Horgby et al., 2019b; Rocher-Ros et al., 2019). In both cases, fluxes are then calculated based on estimated pCO_2 and calculated gas transfer velocities (k) from stream turbulence and geomorphology (e.g., Raymond et al., 2012; Ulseth et al., 2019). While these methods allow for large-scale flux estimates from relatively coarse resolution observations, recent work has suggested that associated flux estimates involve significant uncertainty. These uncertainties include mismatched scales of pCO_2 and k estimates (Lauerwald et al., 2015; Raymond et al., 2013) and observations that are generally biased towards larger stream systems (Sawakuchi et al., 2017). Additionally, a recent analysis of global pCO_2 observations suggests that inverse correlations between pCO_2 and k values may result in large overestimations of stream CO_2 fluxes using traditional statistical upscaling methods (Rocher-Ros et al., 2019); however, the effects of this correlation on flux estimates have not been directly tested.

While models used to predict fluxes are based primarily on statistical measurements, the processes that control stream CO_2 concentrations and fluxes have been characterized in a number of studies (e.g., Duvert et al., 2018; Horgby et al., 2019a; Horgby et al., 2019b; Hotchkiss et al., 2015; Raymond et al., 2012). Concentrations of CO_2 in streams are determined by the balance of inputs, including soil and groundwater CO_2 and respiration of organic carbon within the water column and hyporheic zone, and outputs such as atmospheric evasion and photosynthesis. In terms of spatial variability of CO_2 concentrations, evasion rates control where on the landscape pCO_2 is highest or lowest, as pCO_2 may degas over scales of 10's of meters (Johnson et al. 2009; Lupon et al., 2019). A number of studies have found that k values which control evasion, are primarily related to discharge and topography, allowing for large-scale estimates based on hydrographic datasets (Raymond et al., 2012; Ulseth et al., 2019). While evasion exerts a strong control on the spatial variability of CO_2 concentrations and fluxes (Rocher-Ros et al., 2019), integrated fluxes from stream networks, however, are controlled primarily by CO_2 sources.

Sources of stream CO_2 are broadly categorized as either allochthonous or autochthonous, where allochthonous sources are CO_2 dissolved in soil- and groundwater (GW) that is transported to the stream, and autochthonous CO_2 is produced in the water column or within the hyporheic zone (Marx et al., 2017). While studies have converged on a conceptual model in which autochthonous sources become increasingly important with increasing stream size, the relative balance of these sources remains uncertain. For example, in a survey of USGS NWIS monitoring sites, Hotchkiss et al. (2015) found that while autochthonous contributions increased with stream size, GW was the dominant source across all sites. In contrast, a recent CO_2 budgeting study of 1^{st}-3^{rd} order streams in the Cote Du Nord region found that autochthonous sources accounted for ~75% of stream CO_2 (Rasilo et al., 2017). Thus, the lack of constraints on CO_2 source contributions remains a major knowledge gap in terms of our ability to predict stream CO_2 variability.

Process-based models that incorporate transport and chemical reactions are extremely useful for disentangling complex natural systems and predicting elemental fluxes (Steefel et al., 2005). The processes controlling CO_2 in river systems, including where and how they operate, are relatively well-defined; therefore, we are uniquely poised to incorporate these into a predictive model framework. Due to the spatiotemporal variability of pCO_2 and complex set of reactions that govern its fate and transport, we argue that a stream network model is an ideal method of mechanistically modeling pCO_2 in a manner that allows for pCO_2 to be predicted at the high spatial resolution required to accurately calculate landscape fluxes (Rocher-Ros et al., 2019). Beyond predicting pCO_2 and fluxes, stream network models can help to determine the relative importance of CO_2 pathways into streams comparing potential contributions of water column and hyporheic zone respiration along with GW CO_2 inputs. Additionally, stream network models can be used to identify potential hotspots and hot moments to guide fieldwork. In this study, we develop and apply a stream network model of stream CO_2 to a mountainous watershed in Gothic, CO containing 1^{st}- 5^{th} order streams. We validate this model against a new high-resolution dataset of stream geochemistry. We further compare model results to existing upscaling and multiple linear regression model techniques, and use the model-data comparisons to evaluate the relative importance of internal and external CO_2 sources.

2 Methods

2.1 Field Site Description

This study was conducted in the East River watershed near the Rocky Mountain Biological Laboratory in Gothic, Colorado (USA). The East River watershed delineated at the star shown in Fig. 1 is 87 km^2 and includes 1^{st} to 5^{th} Strahler order streams. The watershed ranges in elevation from 2,760 to 4,123 m above sea level, has a mean slope of 23^o (Winnick et al., 2017), and is broadly representative of watersheds throughout the Rocky Mountains

(Battaglin et al., 2011; Markstrom & Hay, 2009). Snow is the dominant form of precipitation in the basin with an average precipitation of 1.23±0.26 m y^{-1} and an annual average temperature of 1°C (PRISM, 2013). During the sampled period, snow was present in the higher elevations and meltwater was contributing to the discharge (*Q*). The three major life zones within the basin are alpine, montane, and subalpine (Carroll et al., 2018; Hubbard et al., 2018) and the majority of the watershed is underlain by the Mancos Shale formation in which weathering solute fluxes are dominated by calcium carbonate dissolution and pyrite oxidation (R. W. H. Carroll et al., 2018; Morrison et al., 2012; Winnick et al., 2017). However, the western side of the basin have a greater proportion of Quartz Monzonite Porphyry and tributaries display lower solute concentration when compared to the rest of the watershed (Carroll et al., 2018; Gaskill et al., 1967, 1991).

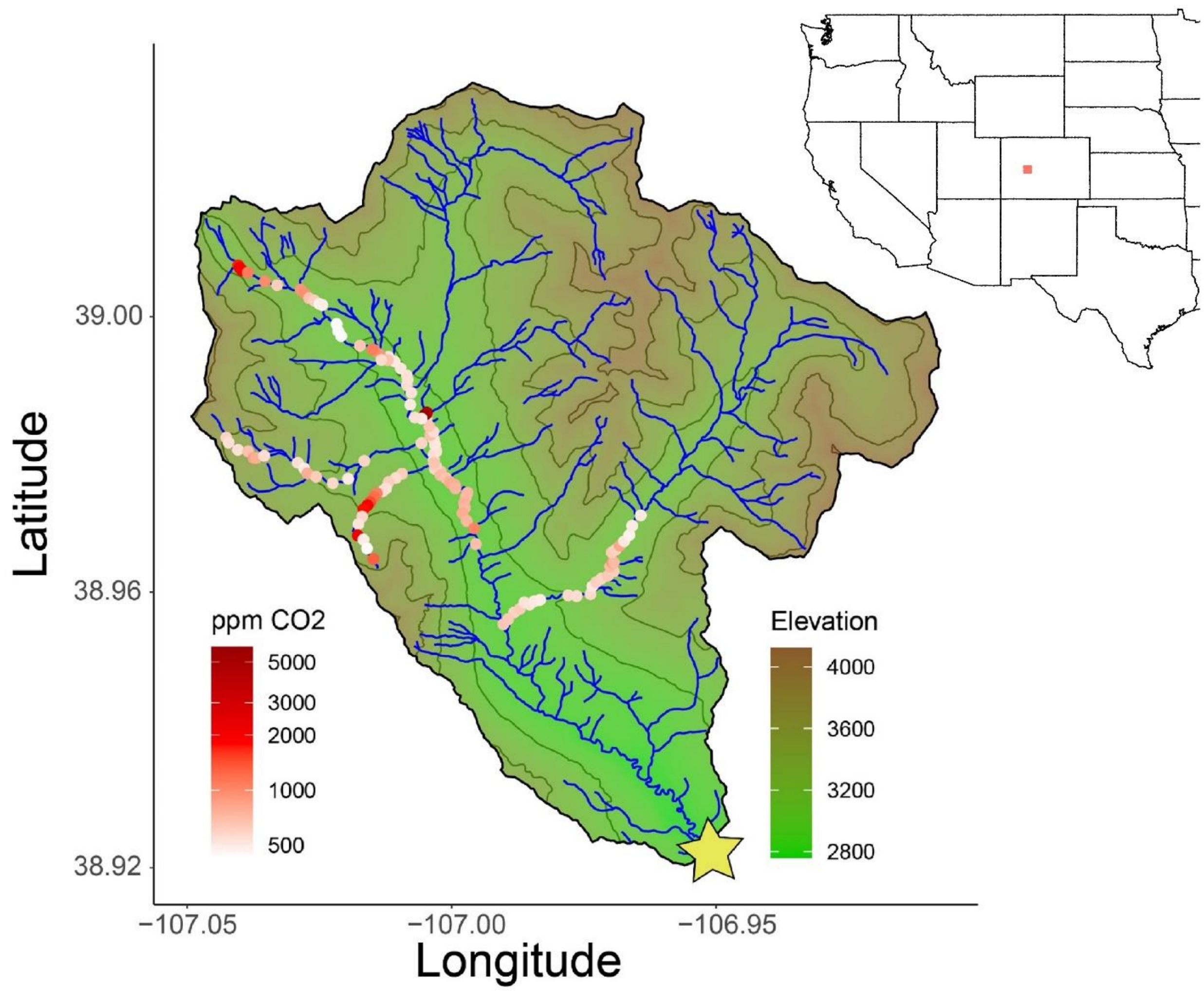

Figure 1: Map of the East River watershed (87 km^2) with NHDplus flow lines of the East River and tributaries shown in blue, shaded elevation contours in green, and field-sampled pCO_2 (ppm) as points colored from low too high in red (n=121).

2.2 Sampling Methods

Geochemical measurements and stream samples were taken across the East River and its tributaries over a 10-day period in August 2019 (Fig. 1). While discharge data for this time period was not available from a proximal gauging station, August discharge values range from 0.43 to 2.81 m^3s^{-1} (2014-2016 and 2018) (star in Figure 1) (Carroll & Williams, 2019) and precipitation during the sampled days totaled 3.3 cm (Newcomer & Rogers, 2020). Samples were taken longitudinally along the stream every ~80 m within the designated reaches. At every site, direct pCO_2 measurements were taken using an EGM-5 Portable CO_2 Infra-Red Gas Analyzer (PP Systems). Samples were prepared by equilibrating 80 ml of stream water with 60 ml of atmosphere in a gas-tight syringe, which was shaken vigorously for 60 s before direct injection into the analyzer. Measurements were corrected for atmospheric CO_2 by calculating the total moles of CO_2 within the sampled air and water at equilibrium then subtracting the moles estimated in the air at a pCO_2 of 400 ppm. Additional measurements such as pH, conductivity, dissolved oxygen (DO), and temperature were taken with a Yellow Springs Instruments (YSI Professional Plus) (n=151).

2.3 Stream Network CO_2 Model

We developed a stream network model based on the advection-reaction equation for solute transport to predict pCO_2 across the East River watershed. These types of models have been recognized as an important method of estimating elemental fluxes by enhancing the spatial and temporal coverage of data (Bencala & Walters, 1983). Changes in CO_2(aq) (C; mol/L) through time (t) are calculated as,

$$\frac{dC}{dt} = -v\frac{dC}{dx} + \frac{1}{A}\frac{dQ}{dx}\left(C_{gw} - C\right) - k_{CO2}(C - C_{atm}) + F_{wc} + F_{he} \quad (1),$$

Table 1: parameters used in the model with "value, Unit" column showing the equation or value used in the model and the "Range" column showing the ranges outputted from the model or the ranges used in the optimization.

Variable	Description	Value, Unit	Range	Data source
C_{atm}	Atmospheric $CO_{2(aq)}$	2.13e-5, mol L^{-1}	-	
C_{gw}	Groundwater $CO_{2(aq)}$	0.0012, mol L^{-1}	0.0006-0.0009	optimization
C_{hz}	Hyporheic $CO_{2(aq)}$	+3.2e-5, mol L^{-1}	1.1e-5-5.3e-5	optimization
$C_{wetland}$	Wetland Groundwater $CO_{2(aq)}$	0.0025, mol L^{-1}	0.0021-0.0027	optimization
DA	Change in area over change in length	m	3.23e-7 -1.05e-4	DEM
D_m	Molecular diffusion coefficient of CO_2 in water	$1.6e^{-9}$, m^2 s^{-1}	-	Grant et al., 2018
eD	Energy dispersion rate of the stream	Eq. 4, m^2 s^{-3}	0-4.95	Horgby, Segatto, et al., 2019
F	Watershed CO_2 fluxes	Eq. 15, Moles C	-	
F_{he}	Hyporheic zone molar fluxes of $CO_{2(aq)}$	Eq. 8, mol L^{-1} s^{-1}	0-0.016	
F_{wc}	Water column molar fluxes of $CO_{2(aq)}$	Sup Eq. X, mol L^{-1} s^{-1}	0-1.8e-5	
g	Gravitational acceleration	9.8, m s^{-2}	-	
h	Stream depth	Eq. 13, m	0.03-0.35	Horgby, Segatto, et al., 2019
K_{600}	Gas transfer velocity corrected to 20 °C	Eq.2/3, m d^{-1}	0-0.20	Horgby, Segatto, et al., 2019
K_{CO2}	Gas transfer velocity of CO_2	Eq. 6, m d^{-1}	0-0.17	Ulseth et al., 2019
k_{hz}	Hyporheic zone gas transfer velocity	Eq. 9, m d^{-1}	0-0.003	Grant et al., 2018
Q	Discharge	m^3 s^{-1}	0.01-1.95	
s	Stream slope	*	0-1.81	DEM
sc_t or sc	Schmidt number	Eq. 5/10, *	834.8 or 812	Grant et al., 2018
T	Temperature	13.7, °C	-	
u	Shear velocity	Eq. 11, m s^{-1}	0-1.5	Grant et al., 2018
v	Stream velocity	Eq. 12, m s^{-1}	0.01-0.85	Horgby, Segatto, et al., 2019
w	Stream width	Eq. 14, m	0.06-6.62	
x	Distance	m	-	

* unitless

where v is velocity (m s^{-1}), A is stream cross-sectional area (m^2), Q is discharge (m^3 s^{-1}), x is lateral distance (m), C_{gw} and C_{atm} are the molarity of CO_2 in groundwater and atmosphere-equilibrated water, respectively (see Table 1 for model variables and descriptions). The molar fluxes of $CO_{2(aq)}$ (mol L^{-1} s^{-1}) from water column and hyporheic zone net respiration are F_{wc} and

F_{he}, respectively (Table 1). To estimate potential water column respiration, F_{wc} is set to a constant rate of 7*10^{-11} (mol L^{-1} s^{-1}), which represents the high end of values found by Ward et al. (2013) in the productive Amazon river as an estimate of maximum potential water column contributions. The reaeration coefficient of CO_2, k_{co2} (s^{-1}), was calculated as the gas transfer velocity of CO_2 divided by stream depth. The gas transfer velocity of CO_2 was estimated using k_{600}, based on the equations of Ulseth et al. (2019):

$$\ln(k_{600}) \text{for eD} > 0.02 = 1.18 * \ln(eD) + 6.43 \quad \text{(2), and}$$

$$\ln(k_{600}) \text{for eD} < 0.02 = 0.35 * \ln(eD) + 3.10 \quad \text{(3).}$$

Here, eD is the energy dissipation rate of the stream (m^2 s^{-3}) calculated as,

$$eD = g * v * s \quad \text{(4),}$$

where g is the acceleration due to gravity (9.8 m s^{-2}), and s is stream slope (unitless, m m^{-1}). In order to convert k_{600} into k_{CO2}, we calculated the Schmidt number sc_t (unitless) using the average daily air temperature T (13.7 ^{o}C) of the sampling period and the equation (Wanninkhof, 1992),

$$sc_t = 1911 - 118.11 * T + 3.453 * T^2 - 0.0413 * T^3 \quad \text{(5).}$$

The k_{CO2} variable was then calculated using the equation (Raymond et al., 2012),

$$k_{CO2} = \frac{k_{600}}{(600/sc_t)^{-0.5}} \quad \text{(6),}$$

where *-0.5* is assumed due to the turbulent surfaces of streams (Jähne et al., 1987; Ulseth et al., 2019).

Equation 1 was solved assuming steady state conditions using a backwards-difference finite approximation scheme,

$$0 = -v\left(\frac{C_i - C_{i-1}}{\Delta X}\right) + \frac{1}{A}\left(\frac{\Delta Q}{\Delta X}\right)\left(C_{gw} - C_i\right) - k_{CO2}(C_i - C_{atm}) + F_{wc} + k_{hz} * (C_{hz} - C_i) \quad \text{(7),}$$

with *i* and *i-1* representing a grid cell and the previous grid cell respectively. From Eq. 1, F_{he} was parameterized using the equation,

$$F_{he} = k_{hz}(C_{hz} - C) \quad \text{(8),}$$

where C_{hz} is the molarity of CO_2 in the hyporheic zone and k_{hz} is the hyporheic zone mass transfer coefficient (m s^{-1}). Using principles of surface renewal theory, k_{hz} was calculated using the parameterization of Grant et al. (2018) as,

$$k_{hz} = 0.17u * sc^{-2/3} \quad (9),$$

where u is the shear velocity (m s^{-1}). The assumption that turbulent mixing is the primary process controlling CO_2 production in the stream bed is supported as the short transit times of the flow paths caused by turbulent mixing are of similar temporal scale to aerobic respiration (Breugem et al., 2006; Harvey et al., 2019). Additionally, the lower data requirements of this assumption allow for the model to be highly scalable. The sc term is calculated as,

$$sc = \frac{kv}{D_m} \quad (10),$$

where kv is kinematic viscosity of water (m^2 s^{-1}) and D_m is molecular diffusion coefficient of CO_2 in water (m^2 s^{-1}). Shear velocity is calculated as,

$$u = \sqrt{ghs} \quad (11),$$

where s is slope (unitless, m m^{-1}), and h is depth (m).

In order to predict pCO_2 across the watershed, we solved Eq.7 for every grid cell sequentially along each reach starting with 1st order streams. The initial C_i in the first grid cell within 1st order streams was set to C_{gw}, and C_i values at stream junctions were calculated as the discharge-weighted mean of all contributing stream model cells. The grid cells were set using flow line vertices from the NHDplus dataset (U.S. Geological Survey, 2019) which resulted in variable grid spacing with 392 stream reaches and 7969 model grid cells. Topographic information for each grid cell such as slope and elevation were retrieved and calculated from a 10m DEM.

Due to ongoing snowmelt in the upper basin that lagged snowmelt in the lower basin, we used elevation to estimate local contributing runoff (m/s) using a linear regression as snow in the high elevations led to increased Q (Sup Fig. 1) (Carroll & Williams, 2019). The change in discharge along stream reach ($\Delta Q/\Delta x$ in Eq. 7) was calculated as local runoff multiplied by the NHDplus reach upstream accumulating area (UAA) per unit length of the stream reach. Discharge at each grid cell was calculated as the discharge at the previous grid cell plus runoff-based groundwater inputs, assuming constant gaining conditions. The stream width (*w*), depth (*h*), and velocity (*v*) in meters were calculated using scaling relationships from Horgby et al. (2019b) for mountainous streams as,

$$v = 0.668 * Q^{0.365} \quad (12),$$

$$h = 0.298 * Q^{0.222} \quad (13), \text{ and}$$

$$w = Q/v/h \quad (14).$$

The calculated *v* along with k_{CO2} was additionally used to determine stream CO_2 half-life at each point using a first order reaction,

$$half\ life = \frac{ln(2)}{k_{CO2}/v} \quad (15)$$

representing the distance over which stream CO_2 evades assuming no additional CO_2 inputs (Sup Fig. 2).

The model was further amended to capture observed field conditions including wetland and snow plug locations. Specifically, wetlands are often sources of elevated CO_2 in groundwater (Buffam et al., 2010; Hope et al., 2004), and snow plugs may act to trap CO_2 in the stream environment by limiting water-atmosphere interfaces. Snow plugs were defined as large areas of snow covering the stream, and modeled k_{CO2} was set to 0 where snow plugs were noted. Stream sections that were within perennially saturated organic-rich fens were modeled using $C_{wetland}$ in place of C_{gw}, and field measurements of standing fen pools indicated pCO_2 above the EGM-5 calibrated range of 25,000 ppm. Lastly, NHDplus headwater flowlines were trimmed to match points of stream emergence recorded in the field.

Within all the above model equations there are only three free parameters: CO_2 concentrations in GW, wetlands, and the hyporheic zone relative to the stream. To tune the model, we simulated the model across variable ranges of 5000-50000, 10000-100000, and 0-2000 for C_{GW}, C_{wet}, and $(C_{hz} – C)$, respectively. We chose the optimized values based on maximum coefficients of determination (R^2) and minimum Root Mean Square Error (RMSE) from model-data comparisons described below. Model R code along with NHDplus hydrography datasets for the basin are included in the Supplemental Information.

2.4 Statistical Analyses

In order to compare the model output to our sampled points, GPS locations of the sampled points were paired with their closest model grid cell. The paired points were filtered to remove any that were more than 50m apart, or for which there was no NHDplus counterpart (n=30). Points without NHDplus counterparts comprised seeps and small streams that were not represented by NHDplus flowlines. The remaining 121 points of which 12, 23, 21, and 65 are 1st – 4th order respectively, were compared using model-data R^2, RMSE, and t-tests to the stream network model with and without benthic respiration (BZ) to determine if the addition of internal processes add predictive power to the model. All calculations were conducted using R (R Core Team, 2020; Supplemental Information).

A multiple linear regression model (MLRM) predicting $p\mathrm{CO_2}$ based on Q, velocity, slope, elevation, and mean watershed net primary production (NPP) (NASA, 2019) was determined using a stepwise approach. Using Q, k_{CO2}, velocity, slope, elevation, stream order, k_{hz}, mean watershed NPP, and landcover as the initial inputs, all possible regression combinations were calculated. The best regression model was chosen based on the lowest AIC value that contained only significant predictors ($p<0.05$). The final regression was evaluated by calculating the mean and variance of the $p\mathrm{CO_2}$ predicted as well as comparing the R^2 and RMSE values. Additionally, global scale mountainous inland water CO_2 fluxes were recently estimated using an MLRM based on $p\mathrm{CO_2}$ data in the European Alps (Horgby et al., 2019b). The regression consisted of elevation, Q, and soil organic carbon (SOC) from Hengl et al. (2017). For comparison, we applied this model to the East River watershed to test the potential scalability of the Horgby MLRM to different field areas.

Additionally, we compared existing statistical upscaling methods for estimating watershed-scale CO_2 fluxes based on point measurements to integrated model output. Two common methods of upscaling CO_2 evasion fluxes were evaluated against the stream-network modeled fluxes. The flux estimation methods evaluated used Eq. 16 and the same k_{CO2}, h, w, and Δx as the stream network model. In the upscaling models, $p\mathrm{CO_2}$ was calculated as 1) mean $p\mathrm{CO_2}$ from all samples across the watershed; and 2) mean stream $p\mathrm{CO_2}$ by Strahler order (Butman & Raymond, 2011; Raymond et al., 2013). The corresponding CO_2 fluxes were compared to stream network model fluxes for each stream order. The watershed-scale CO_2 evasion fluxes (F) were calculated for the modeled and regression data using the equation,

$$F = \sum(C_i - C_{atm}) * k_{CO2} * h * w * \Delta x \quad (16).$$

Additionally, we repeated the upscaling methods with flux estimates restricted to the reaches with sampled data to evaluate model and upscaling performance within well-characterized areas.

3 Results

3.1 Observational Data

Stream waters across the East River and its tributaries had a mean temperature of 8.1 ^{o}C ranging from 2.7 – 14 ^{o}C at elevations ranging from 2873 – 3521 m. Across all sample points, the mean dissolved oxygen (DO) was 91% and ranged from 0.4 – 11.4 mg L^{-1}. The mean pH was 8.03 ranging from 7.14 – 8.4. Roughly 90% of samples were below 8.3, such that bicarbonate was the dominant inorganic carbon species present. Conductivity within the data ranged from 11.6 – 263.1 μs cm^{-1} with a mean of 112.4 μs cm^{-1}.

Measured pCO_2 was consistently elevated above atmospheric concentrations with a mean of 820 ppm and range of 433-6044 ppm (Fig. 1). First order streams had the highest mean pCO_2 at 1963 ppm. Increasing stream order generally corresponded to decreasing mean pCO_2, with 2^{nd}-4^{th} order streams having mean pCO_2's of 952, 616, and 628 ppm respectively. The minimum pCO_2 within each order showed little variation, ranging from 433-527 with no correlation to stream order; however, the maximum values decreased with increasing stream order with a pCO_2 of 6044, 2074, 1090, and 1040 ppm in 1^{st} – 4^{th} order streams respectively. Additionally, k_{CO2} was found to restrict in-stream pCO_2 as 95% of sampled points with k_{CO2} values of greater than 0.005 (m/s) had pCO_2<1000, similar to findings in a Swedish catchment system (Fig. 2) (Rocher-Ros et al., 2019).

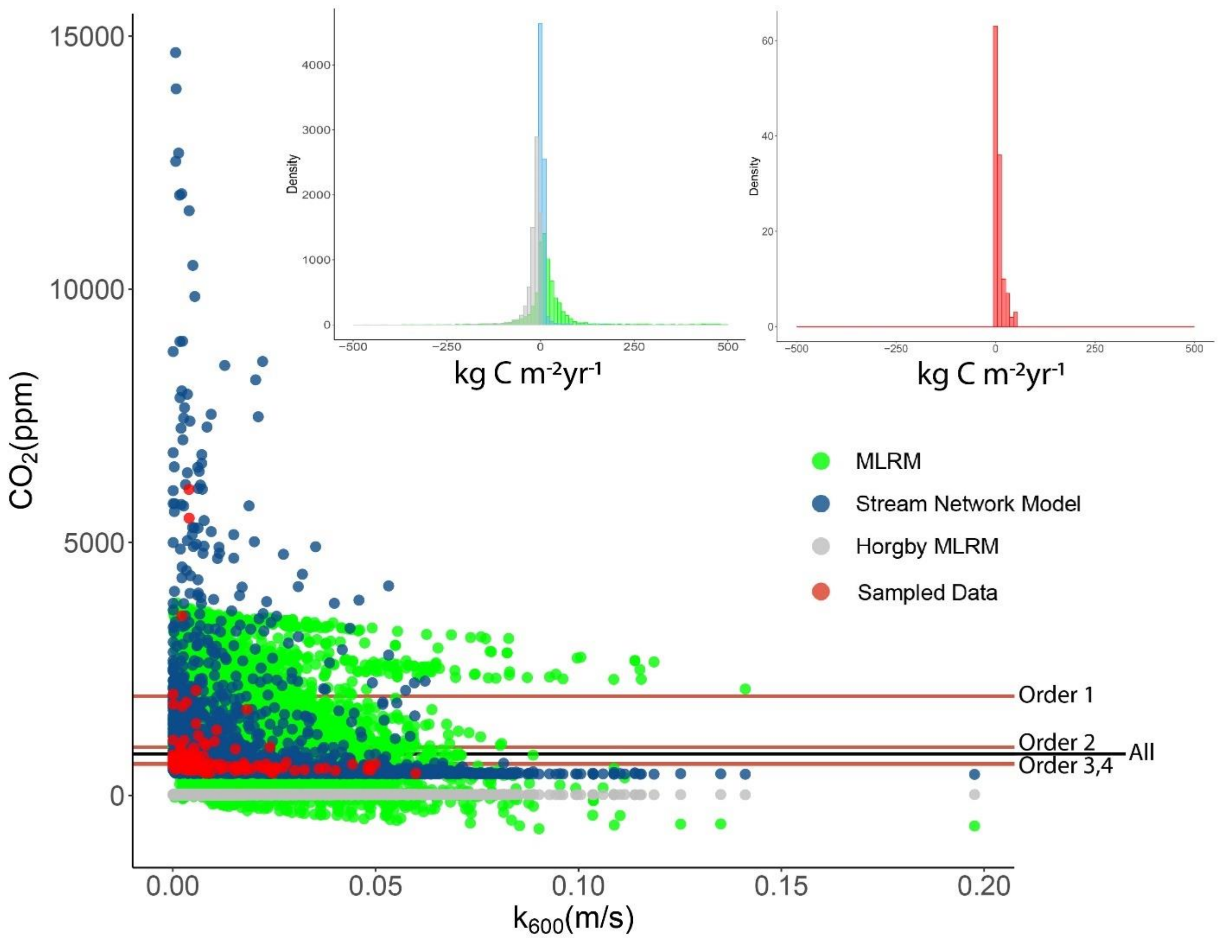

Figure 2: Stream pCO$_2$ plotted against k_{600} in m/s with MLRM in green, stream network model in blue, Horgby MLRM in gray, and sampled data in red. Lines show values used in the upscaling calculations with brown lines representing mean pCO$_2$ in 1st – 4th order streams top to bottom and the black line is the mean of all sampled pCO$_2$. Histogram of fluxes are shown in the inset with sampled data shown separately so variability can be seen.

Point sample data was used to estimate total watershed CO$_2$ fluxes based on two separate upscaling methods as described above (Butman & Raymond, 2011; Raymond et al., 2013). The first method used the mean sampled pCO$_2$ and applied it across the entire stream model using the modeled stream morphology and k_{CO2}, which resulted in total watershed fluxes of 6.4$\pm$11.6 Gg C yr^{-1} (Raymond et al., 2013). The second method was to predict CO$_2$ fluxes separately for each stream order using the mean pCO$_2$ within each order as the orders CO$_2$ concentration while maintaining the other modeled parameters. This predicted pCO$_2$ fluxes of 6.3$\pm$5.8 Gg C yr^{-1} with

1st-5th orders contributing 2.7±3.5, 0.9±0.8, 0.4±0.4, 0.8±0.4, and 1.5±0.8 Gg C yr^{-1}, respectively. Additionally, flux predictions were restricted to the 2508 m of sampled reaches out of the total 164872 m in the east river. This was done in order to compare upscaling methods to sampled data on a one-to-one basis (Table 2). This resulted in a prediction of 0.06 Gg C yr^{-1} released from the sampled reaches based on measured data, 0.15 Gg C yr^{-1} based on mean pCO_2, and 0.09 Gg C yr^{-1} based on mean pCO_2 by order showing that the signal mean method predicted fluxes 2.5x more than sampled data and the mean by order method predicted 1.5x the fluxes of sampled data.

Table 2: model performance with RMES and R^2 for the full data range and R^2 by order. Predicted range of $p\,CO_2$ and CO_2 flux are shown for each model for the entire watershed and only within the sampled reaches.

	$p\,CO_2$ range(ppm)	R^2	P	RMSE	R^2 1st order	R^2 2nd order	R^2 3rd order	R^2 4th order	Fluxes Gg C/yr	Sampled reach Fluxes Gg C/yr
Sampled data	433 - 6044	-	-	-	-	-	-	-	-	0.06
Stream network Model	416 - 18000	0.7	$<10^{-15}$	763	0.71	0.57	0.49	0.34	1.3	0.03
MLRM	-660 - 3804	0.25	$<10^{-8}$	518	0.75	0.03	0.01	0.17	17.7	-
Horgby MLRM	12 - 32	0.27	$<10^{-12}$	1106	0.79	0.03	0	0.02	-5.9	-0.14
Upscaling by Mean $p\,CO_2$	820	-	-	-	-	-	-	-	6.4	0.15
Upscaling by Mean order $p\,CO_2$	628 - 1963	-	-	-	-	-	-	-	6.3	0.09

3.2 Model Results

The optimization of the model resulted in a C_{GW} pCO_2 of 18,000 ppm, C_{wet} pCO_2 of 44,000 ppm, and a hyporheic zone pCO_2 elevation $(C_{hz} - C)$ of 600 ppm. The best three optimizations runs all had the same C_{GW} value, which falls within the range of sub-soil (>30 cm) growing season pCO_2 values measured in a soil profile within the East River (~7,000 – 23,000 ppm; Winnick et al., 2020). Wetland pCO_2 measured in the East River was above the 25,000 ppm calibration of the EGM-5 supporting the elevated model optimization value. The hyporheic zone pCO_2 was found to be elevated above stream pCO_2 by 600 ppm which was at the upper range (~0 – 700 ppm) (Sup Fig. 3) of values calculated from measured pH and estimated alkalinity (Nelson et al., 2019).

The full model predicted pCO_2 values and captured observed spatial patterns with a RMSE of 763 ppm, R^2 of 0.70 ($p<10^{-15}$) for $\ln(pCO_2)$, and a paired t-value of 0.30 (df=120, p=0.76) for pCO_2 when compared to observed data (Fig. 3). The GW-only stream network model had an RMSE of 1008 ppm, and R^2 of 0.69 ($p<10^{-15}$) for ln(pCO_2), and paired t-value of 0.34 (df=120, p=0.74) for pCO_2. The paired t-test suggests a mean underestimation of 31 ppm between matched points for the GW-only model and 21 ppm for the full model with neither model showing significant difference (p>0.05) from the observed pCO_2 values. As the Full model outperformed the GW-only model in all three metrics of validity, from this point on we will refer to the full model.

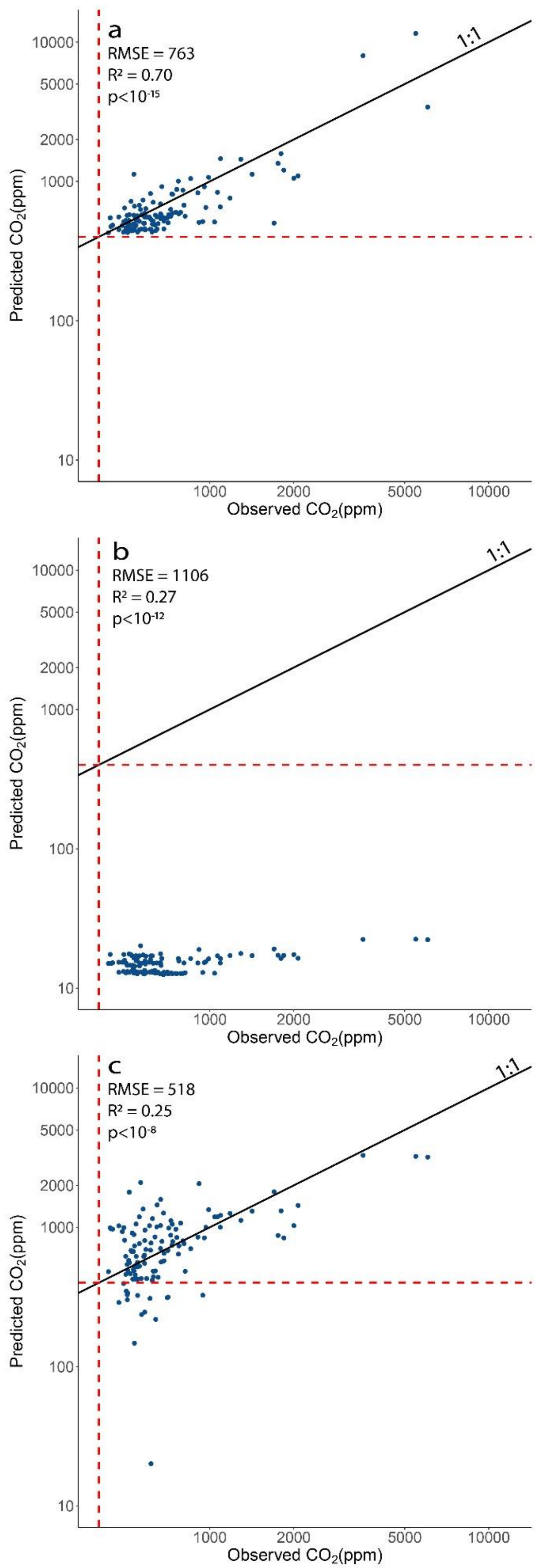

Figure 3: Model-data comparisons and statistics for the (a) stream network model; (b) Horgby MLRM; and (c) MLRM with 2 points missing as they were negative. The dashed lines (red) represent atmospheric

Stream network model pCO_2 was consistently elevated above atmospheric concentrations ranging from 416 ppm to optimized GW values with a mean of 1087 ppm, compared to the measured range of 433-6044 ppm (Fig. 4). The largest discrepancy between the model and the sampled data were at highest observed pCO_2 locations; however, 95% of modeled points were within 400 ppm above and 950 ppm below the sampled points. The highest pCO_2 values were predicted in the headwaters at points of spring emergence and quickly approached atmospheric values. Across all model points, the median calculated CO_2 half-

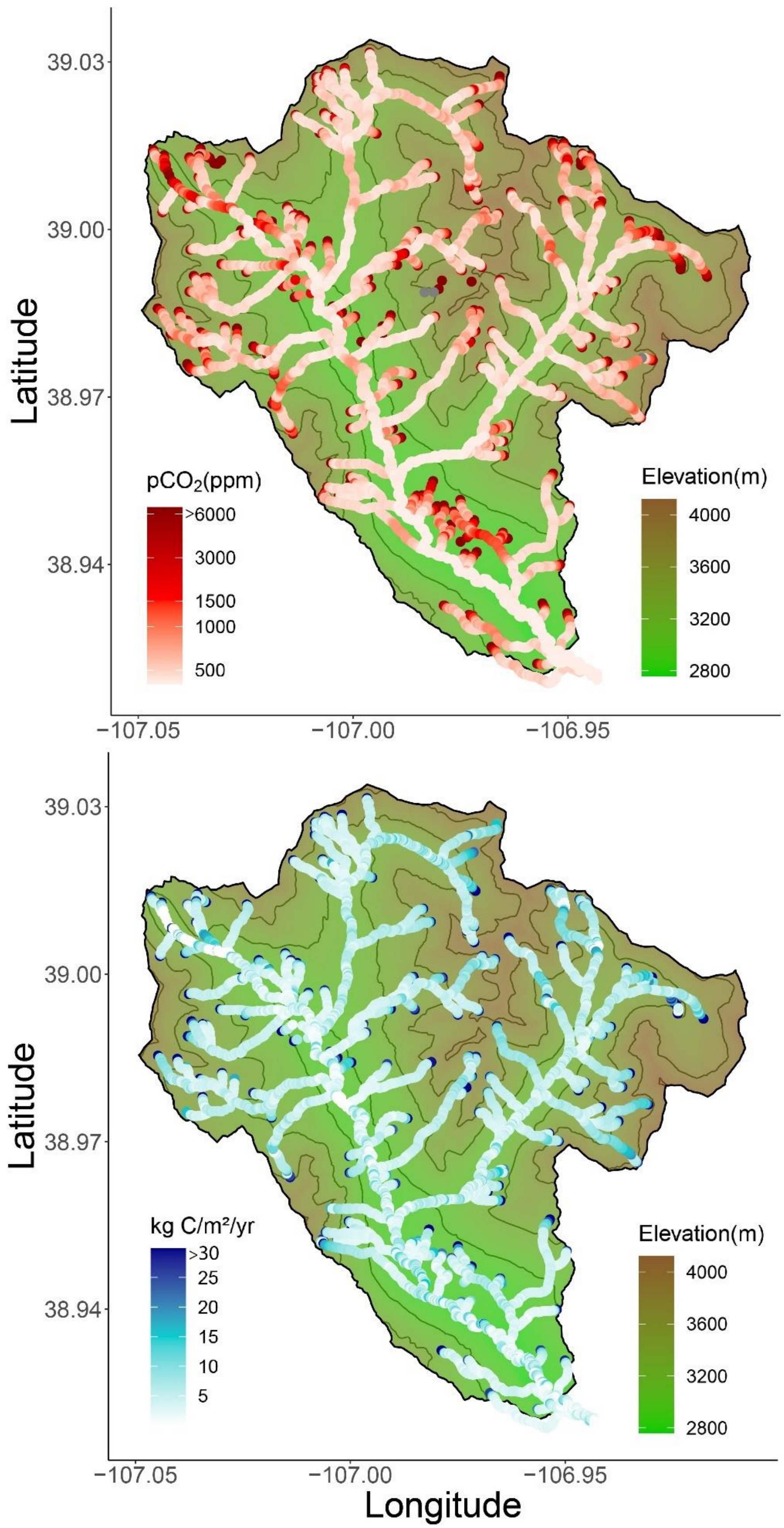

Figure 4: (A) Stream network modeled pCO_2 in the East River shown in red; (B) Stream network model area-normalized CO_2 fluxes shown in blue with fluxes >30 kg C/m^2/yr shown in black (~1% of stream at locations of stream emergence only)

life was 11 m. As a result, model pCO_2 was strongly restricted by k_{CO2}; 95% of sampled points with k_{CO2} values of greater than ~0.005 (s^{-1}) had pCO_2<1000 ppm (Fig. 2).

Modeled patterns were similar to observational data with mean pCO_2 decreasing as stream order increased: 1st-5th order streams had a mean pCO_2 of 1835, 704, 578, 524, and 468, respectively. Similarly, the max *p*CO2 showed a decreasing pattern with stream order with 1st -5th orders having 18000, 8767, 2612, 879, and 535 ppm, respectively. The minimum pCO2 showed no pattern across orders with 1st -5th order streams having 430, 416, 421, 419, and 419 ppm respectively.

The full stream network model predicted a mean flux of 6.3 kg C m^{-2} yr^{-1} ranging from 0 - 448 kg C m^{-2} yr^{-1} with total watershed fluxes at 1.3 Gg C yr^{-1} (Fig.4, Table. 2). The highest fluxes were predicted in first order reaches totaling 0.4 Gg C yr^{-1} with mean area-normalized fluxes of 9.3 kg C m^{-2} yr^{-1}. Total fluxes showed a decrease with order until the 3rd order, at which point fluxes increased with order releasing 0.44, 0.20, 0.19, 0.22, and 0.26 Gg C yr^{-1} in 1st-5th order stream respectively. The stream network model suggests that GW is the largest source of CO_2 in river systems accounting for 53% of CO_2 emitted, followed by benthic respiration at 47%, and water column respiration at 0.1% (Fig. 5). Absolute GW fluxes show a weak negative correlation with Q (R=-0.1) whereas benthic respiration showed a strong positive correlation (R=0.47) with Q. In first order streams, GW contributed 86% of the C fluxes whereas benthic respiration contributed 14%. In the fourth and fifth order streams benthic respiration was 72% and 91% of the fluxes compared to the 28% and 8% contributed by GW (Fig. 6). We note that while precise percent contributions are highly dependent on optimized C_{HZ} values, this overall pattern is a robust feature of the stream network model matching conceptual models of stream CO_2 sources.

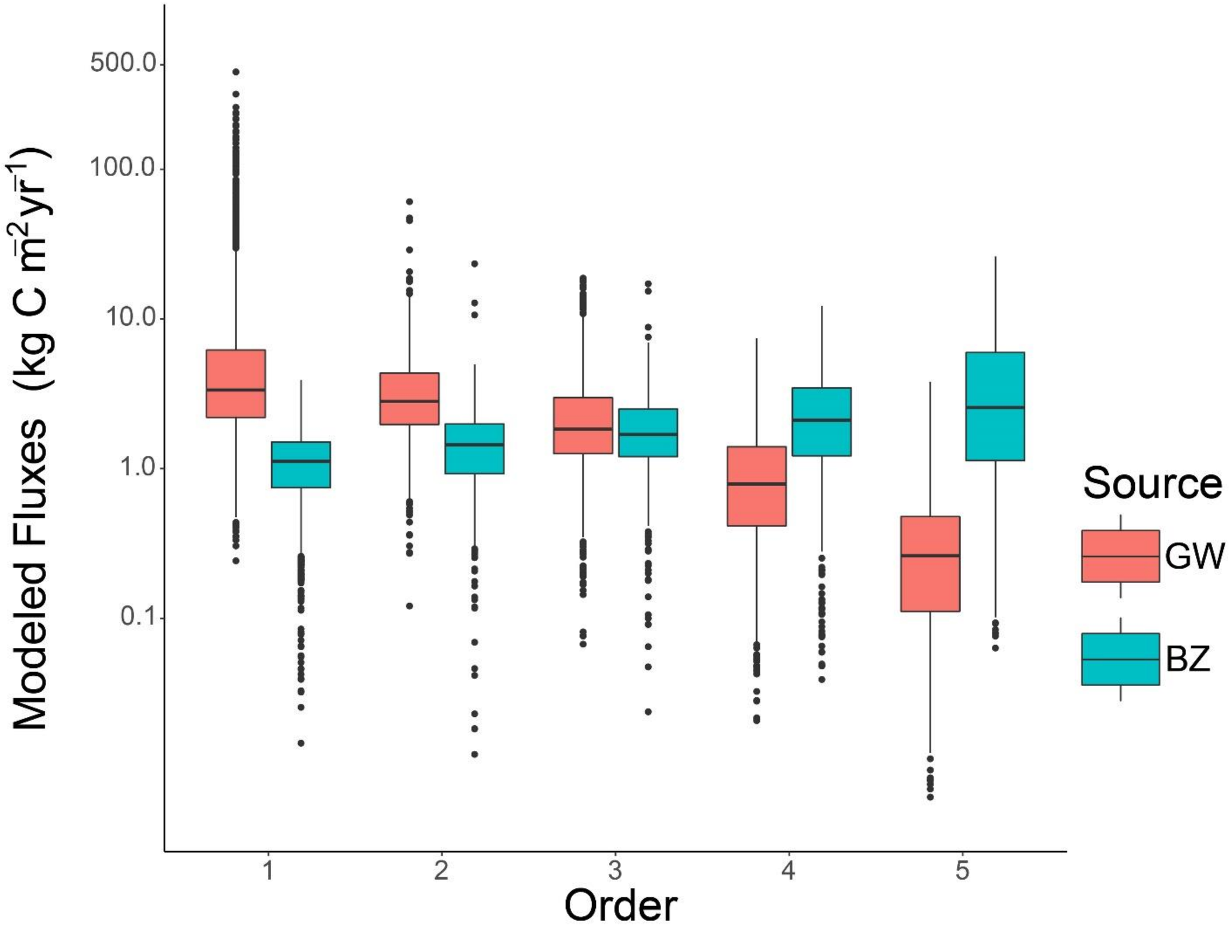

Figure 5: Area-normalized model fluxes from first through fifth order streams with red (left) box representing groundwater contributions and blue (right) representing benthic zone respiration contributions of CO_2. 86 points not shown <0.005.

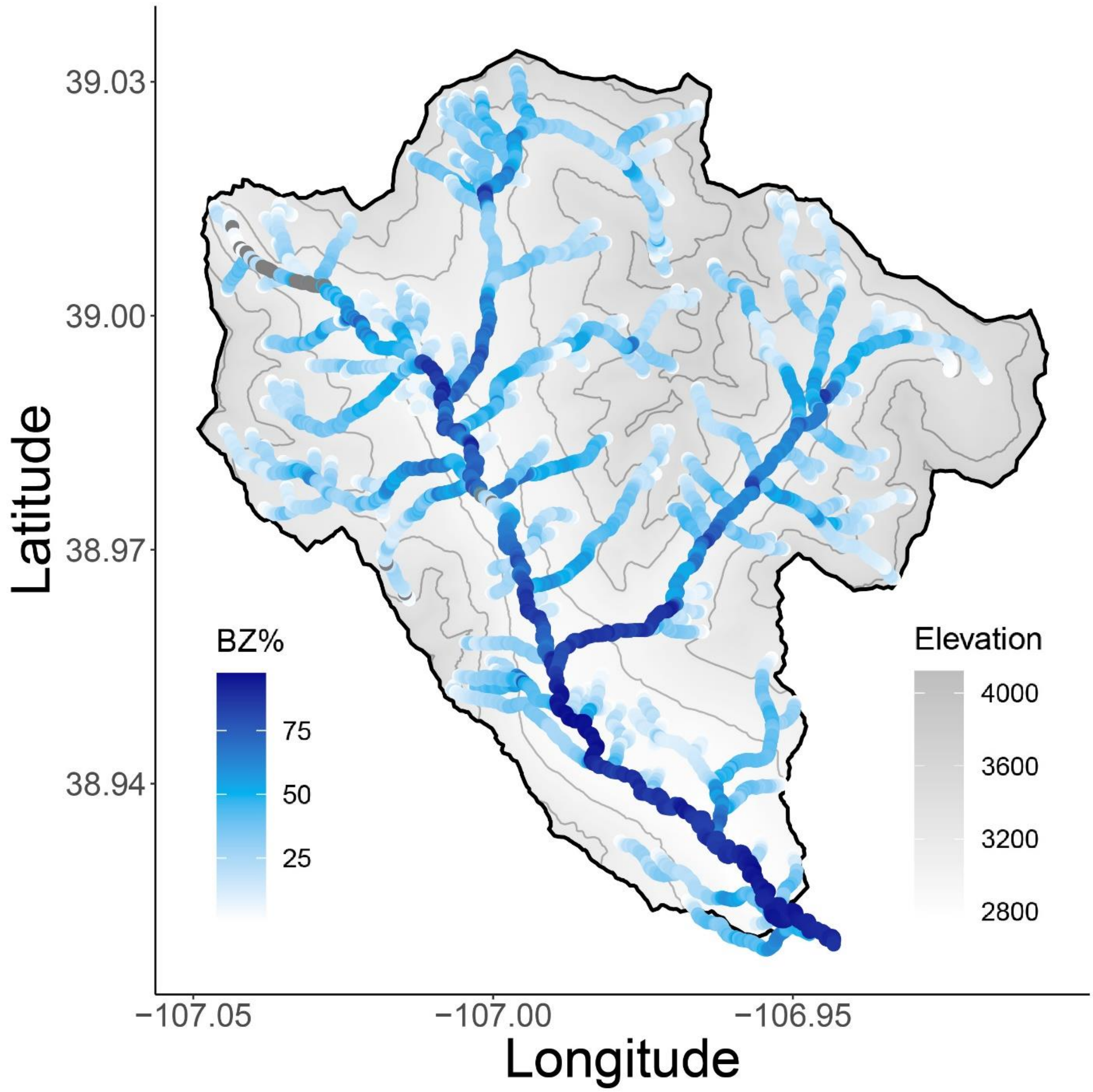

Figure 6: Modeled % benthic zone (BZ) respiration CO_2 contributions at each stream location.

The model suggests that 11% of the East River by length has a CO_2 flux greater than 10 kg C m^{-2} yr^{-1} (Fig. 7), with 78% of these hotspots in 1st order streams and only 4% in 5th order streams. However, as headwaters are a disproportionate length of the stream, we compared the % hotspots within each order to the total stream length of that order. We found that 1st orders are 17% hotspots and that 5th order streams had the second largest proportion of hotspots at 9% with 2nd, 3rd, and 4th having 4%, 6%, and 4% respectively. Hotspots throughout the East River and within each order had significantly higher slope then the mean of the total network or of the respective order. Groundwater dominated hotspots in 1st – 3rd order streams with the BZ contributing 7%, 20%, and 16% respectively whereas BZ respiration was a greater % of CO_2 fluxes in 4th and 5th order streams at 74% and 93% respectively (Sup Table. 1).

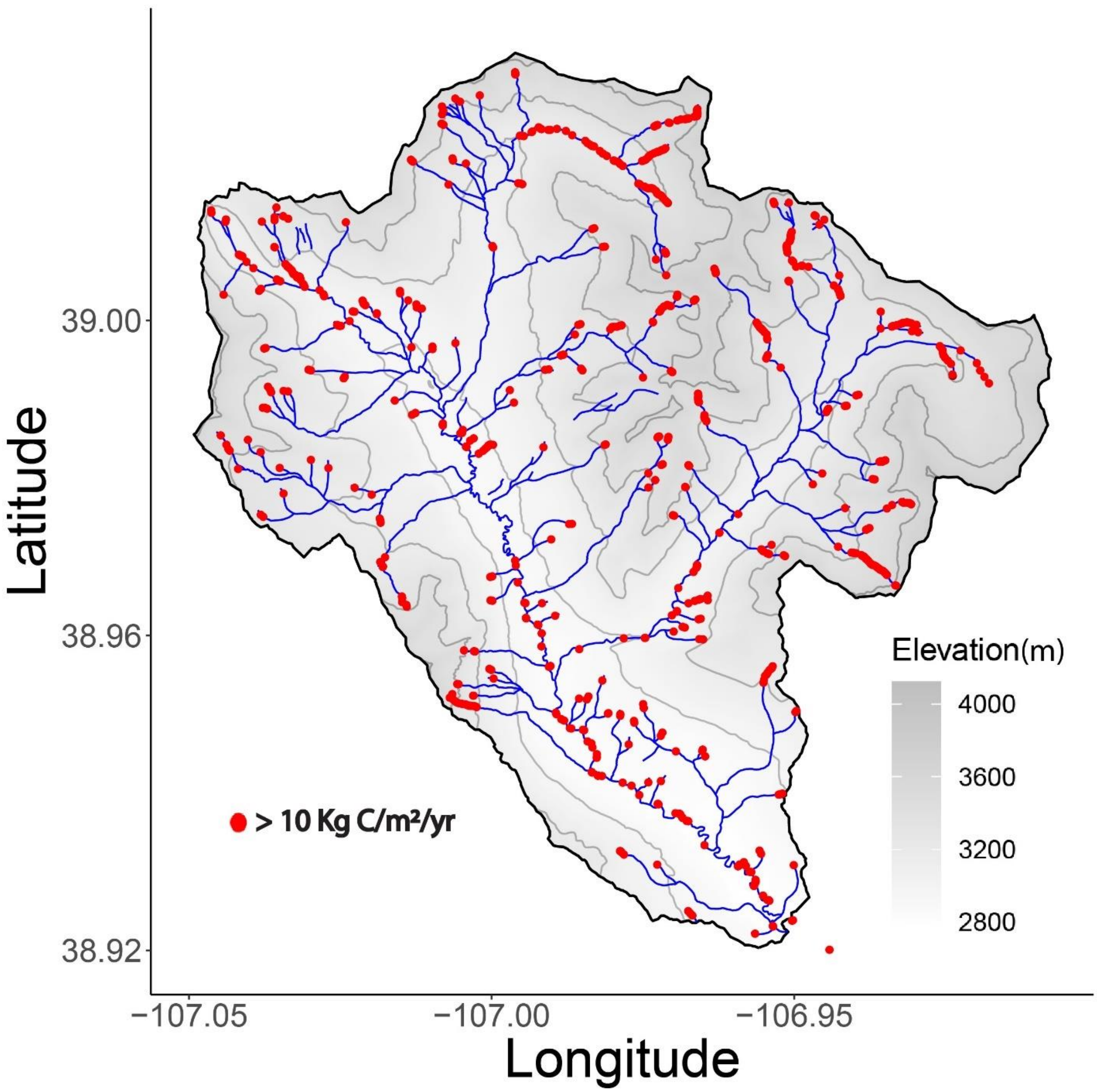

Figure 7: Map of modeled CO_2 flux hotspots. Stream points with area-normalized fluxes greater than 10 kg C m^{-2} yr^{-1} are shown in colored points with streamlines shown in blue.

The stream network model outperformed the stepwise MLRM which found Q, velocity, slope, elevation, and mean watershed NPP to be the only significant predictors of pCO_2 (C_{MLRM}), hence referred to as the MLRM. The MLRM

$$C_{MLRM} = 3599.479 * Q - 8726.124 * v - 1226.308 * s - 3.409 * e - 4.184 * NPP + 14817.114 \quad (17).$$

predicted $\ln(pCO_2)$ with a R^2 of 0.25 ($p<10^{-8}$) and a RMSE of 518 (Fig. 3). The RMSE of the MLRM is better than the stream network model as the MLRM preferentially fits the higher pCO_2 values; however, the low R^2 shows that it is worse at predicting pCO_2 variability, particularly below ~1500 ppm, to the point that negative values are predicted within 2.6% of the East River. Alternatively, the higher RMSE of the stream network model is due to the difficulty in fitting the higher pCO_2 values which is likely due to sensitivity of stream emergence location and spring velocities. Additionally, the MLRM predicted a smaller range of pCO_2 -660 – 3804 ppm than the observed data and stream network model. Using the MLRM across the east river watershed resulted in an estimated CO_2 flux of 17.7 Gg C yr^{-1} (18.3 Gg C yr^{-1} when excluding negatives) with a mean area normalized flux of 38.5 kg C m^{-2} yr^{-1} (Table 2).

The MLRM used in Horgby et al. (2019b), hence referred to as the Horgby MLRM, was compared to observations and showed less accuracy when predicting $\ln(pCO_2)$ with an R^2 of 0.27 $p<10^{-12}$ RMSE of 1106 (Fig. 3), below the R^2=0.39 $p<0.001$ presented in the original paper. Importantly, the Horby MLRM predicts sub-atmospheric pCO_2 values across the watershed in direct contrast with observations. When used to calculate fluxes, this method therefore predicts the East River to be a CO_2 sink, sequestering 5.9 Gg C yr^{-1} (Table 2) with an area-normalized mean of 17.7 kg C m^{-2} yr^{-1}, which is within the 0 - 27 kg C m^{-2} yr^{-1} predicted to be sequestered in the region in the original paper. Additional disadvantages of these linear regression models are that the soil organic carbon map is at courser resolutions (250 m^2) (Hengl et al., 2017) than available DEMs.

4 Discussion

4.1 Stream network models versus statistical predictions of pCO_2

To the best of our knowledge this paper represents the first stream network model to predict pCO_2, although the methodology is similar to previous nitrogen stream network models (Gomez-Velez et al., 2015; Gomez-Velez & Harvey, 2014). Here we show that using a high-resolution 10m DEM and estimated groundwater pCO_2, we are able to predict stream pCO_2 at sub-100 m (22 m mean distance between points) resolution across NHDplus flowlines. Notably, the model is able to capture structural characteristics of stream CO_2 observations that emerge naturally from the representation of physical processes. These include (1) GW CO_2 hotspots based on spring emergence and topographic convergence, in which stream CO_2 decays over spatial scales of ~10¯10^2 m depending on the balance of advection and gas exchange (Fig. 4); (2) diminishing influence of GW inputs with increasing stream size (Fig. 6); (3) atmosphere-super-saturated CO_2 in higher-order streams from stream corridor CO_2 production (Fig.'s 4,6); and (4) inverse correlations between gas exchange velocities and pCO_2 (Fig. 2).

This ability to capture the qualitative structure of spatial variability is borne out by significantly stronger model-data correlations for the stream network model (R^2=0.70) versus the MLRM (R^2=0.25) and Horgby MLRM (R^2=0.27). This structural advantage is even more pronounced when comparing model-data correlation within Strahler stream order. The stream network model predicted ln(pCO_2) in 1st -4th order streams with a R^2 of 0.71^*, 0.57^*, 0.49^*, and 0.34^* respectively compared to the MLRM's R^2 of 0.75^*, 0.03, 0.01, and 0.13^* in first to forth order streams, asterisk denote significance (Table 2). This shows that the stream network model has an improved ability to predict pCO_2 especially within higher order streams as it has improved resolution at lower concentrations. While the MLRM features better RMSE values compared to the stream network model, this is due to the bias of linear regression models to capture extreme values associated with spring emergence as demonstrated by the high model-data R^2 value for 1st order streams. Additionally, the MLRM did not correlate with data from 2nd and 3rd order stream further showing its inability to accurately predict CO_2 at lower concentrations, to the point that negative values are predicted across 2.6% of the East River.

One of the primary reasons MLRM's are unable to capture the structure of stream CO_2 variability across and within stream orders is the implicit treatment of each stream location pCO_2 as independent. In reality, pCO_2 at any given location within the stream network represents a combination of local processes and upstream history. Additionally, the inability of MLRM's to capture realistic patterns outside of training datasets (negative pCO_2 values from the MLRM and sub-atmospheric pCO_2 from the Horgby MLRM) suggests that empirical relationships between landscape variables and local pCO_2 involve a large degree of non-stationarity, limiting their potential transferability or scaling potential. This can be seen in the MLRM as negative values were most common in 1st – 3rd order streams with 30%, 18%, and 48% of negative predictions respectively, and all negative values were predicted above an elevation of 2958 m. The Horgby MLRM is strongly dependent on elevation, with sub-atmospheric values predicted above ~3000 m in the original paper (Horgby et al., 2019b). We suggest that this may relate to vegetation in the European Alps versus the Colorado Rockies, in which a lack of high elevation organic matter may limit allochthonous CO_2 sources in the Alps.

As the stream network model represents physical processes, it has the potential to be highly transferable across sites, which will be tested in future research. Notably, data requirements for the stream network model are roughly equivalent to MLRM's and existing estimation methods of gas transfer velocities (e.g., Raymond et al., 2012; Ulseth et al., 2019). In this application, we used stream data observations to optimize free parameters including GW, wetland, and hyporheic zone pCO$_2$; however, the model may be supplemented in future studies with site-specific measurements of these quantities or empirical models to estimate how these parameters vary across environments. Overall, we argue that the stream network model framework represents a significant improvement over existing empirical methods for estimating stream pCO$_2$.

4.2 Implications for global stream CO_2 fluxes

The improved resolution and pCO$_2$ estimation of the stream network model allow for a more robust estimation of CO_2 fluxes from the East River. Upscaling methods predicted CO_2 fluxes to be ~5x larger than the stream network model. The elevated predictions from statistical upscaling methods likely stem from an overestimation of pCO$_2$ in reaches with high k_{CO2} as the estimated CO_2 concentrations are likely higher than would be expected at these locations (Fig. 2). Additionally, the structure of pCO$_2$ data lends itself to further overestimation as it commonly is right-skewed with few large CO_2 concentrations causing the mean and median to be larger than the mode (Sup Fig. 4). As described above, the Horgy MLRM estimates the East River as a CO_2 sink, which suggests their estimates of global mountainous stream CO_2 fluxes may be artificially low. The MLRM predicted a CO_2 flux 13x greater than the stream network model even though 13% of the model was predicted to be a CO_2 sink, this is likely due to the prediction of pCO$_2$ values in the 2000s at relatively high k_{600} >0.06 m/s (Fig. 2) as hypothesized by Rocher-Ros et al. (2019). The overestimation of CO_2 fluxes seen here confirm that spatial mismatches between model variables represent an important issue in current stream CO_2 emission estimates.

Taken together, these analyses support the idea that current global budgets may significantly overestimate CO_2 fluxes from rivers and streams. While site-based discrepancies between upscaling and MLRM versus stream network fluxes are high (500-1300%), we note that these discrepancies are likely maximized due to the mountainous terrain and elevated gas exchange velocities. Future work will the target the impact of k-$p$$CO_2$ inverse correlations in lowland environments and at regional to global scales. Notably, this may result in a significant downward revision in global stream CO_2 estimates, as has recently been suggested (Rocher-Ros et al., 2019).

4.3 Internal production vs external inputs

The proportion of external and internal sources of CO_2 fluxes in streams is an active area of research, as relative contributions from GW, the soil zone, water column respiration, and the hyporheic zone remain uncertain. Quantifying internal and external sources of CO_2 is difficult and requires extensive field experiments to create C budgets for individual reaches (e.g. Rasilo et al., 2017). This has reduced our broader understanding of CO_2 sources as these field and data intensive studies do not sufficiently cover the range of stream orders, discharges, or landscape characteristics that control the processes contributing to stream CO_2. However, using the full stream network model, we are able to estimate the proportions of CO_2 from internal and external sources that are consistent with field observations from the East River and larger-scale data compilations.

As described above, the model predicts diminishing influence of GW inputs with increasing stream size, consistent with previous studies (Hotchkiss et al., 2015). Additionally, the stream network model suggests that water-column respiration contributes minimally to stream network CO_2 fluxes. This result occurs despite the use of relatively high water-column respiration rates throughout the watershed, and is consistent with the budget analysis of Rasilo et al. (2017) for 1st-3rd order streams in the Cote du Nord region. We note that water-column respiration likely becomes increasingly important at larger stream sizes as has been noted for N_2O production (Marzadri et al., 2017).

Our stream network model further suggests that hyporheic zone respiration within stream benthic layers is the primary source of CO_2 in 4th and 5th order streams, consistent with Rasilo et al. (2017) and contrasting with Hotchkiss et al. (2015). We note that model-data statistical agreement is relatively insensitive to the precise value of hyporheic zone pCO$_2$ used, which itself is likely highly variable across the East River; however, our optimized value agrees well with previously published benthic zone pore water geochemistry from the main stem of the East River (Nelson et al., 2019; Supplementary Information). Despite its potential role in controlling higher-order stream CO_2 concentrations and fluxes, very few studies have sought to characterize the dynamics hyporheic zone carbon production, which instead have focused primarily on nitrogen and oxygen dynamics. Thus, an improved understanding of hyporheic zone CO_2 production and exchange is strongly needed to accurately estimate stream CO_2 concentrations and fluxes.

Although overarching patterns of decreasing external contributions with order hold across the range of modeled HZ pCO_2, a mosaic of BZ and GW dominated sections exist within mid order stream showing that small scale variability plays an important role. This can be seen most readily within 3rd order streams where 60% of the stream length is GW-dominated (Fig. 5,6). In 2nd and 4th order streams we see less extreme patchiness with 85% and 6% of streams by length GW dominated respectively. This emphasizes that local conditions may deviate from predicted patterns, as these transitions within stream systems represent a patchwork dynamic rather than a smooth gradient.

4.4 Hotspots

The magnitude and spatial distribution of carbon fluxes has been the focus of many studies, which have found headwaters to be hotspots of CO_2 fluxes, defined here as locations with CO_2 fluxes greater than 10 kg C m^{-2} yr^{-1}. More recent studies have begun to characterize the interplay of topographically driven evasion and sources of CO_2 which create a mosaic of fluxes and hotspots through stream systems (Duvert et al., 2018; Rocher-Ros et al., 2019). In the past, upscaling and coarse resolution MLRM's have hindered our ability to parse out where in landscapes these hotspots are. Using the stream network model, we are able to predict where in the landscape these hotspots are and their relative contribution to integrated fluxes across stream orders. From this we can see that first order streams are the largest contributors making up 78% of the East Rivers hotspots (Fig.7) agreeing with findings from Duvert et al. (2018) which shows that headwaters are hotspots of CO_2 evasion. However, 5th order streams feature higher proportional hotspot areas as compared to 2nd-4th order streams, making 5th order streams a potentially important source of CO_2 fluxes. Although 5th order streams may have more hotspots then previously surmised, they are still of a smaller magnitude then 1st order streams as the total fluxes were still greater in 1st order streams.

Hotspots in the East River were more likely to be in GW dominated sections, with 93% of hotspots by length receiving greater than 50% of their CO_2 from GW. Comparatively, only 75% of the East River length was GW-dominated. This pattern of GW-supplied hotspots held in 1st – 3rd order streams but inverted in 4th and 5th order streams where hotspots were more likely to be in locations where CO_2 was dominantly supplied by BZ respiration. The location of this inversion has additional significance as 3rd - 4th order streams are where the switch from GW to BZ dominated inputs occurs, showing that hotspots are not purely groundwater supplied but instead can be supplied through internally produced pCO$_2$. Additionally, the mean slope of hotspots is steeper than the mean stream slope of the East River showing that hotspots likely occur in areas of transition from low to high slopes where CO_2 that has built up in low slope reaches is quickly lost when k increases, similar to previous findings (Rocher-Ros et al., 2019). As stream network models are able to predict hotspots and parse out CO_2 sources and topographic controls in actual stream environments, they may further provide the ability to guide target field sampling.

5 Conclusions

Predicting regional and global stream CO_2 emissions remains challenging, and estimates continue to change due to additional sources of data and methodological improvements (Drake et al., 2018). Many of these improvements have additional sources of error including mismatches between data resolution which can become a significant when upscaling (Rocher-Ros et al., 2019). Here, we tested the ability of a stream network model to improve predictions of stream CO_2 concentrations and fluxes through representation of physical hydrologic processes, including atmospheric gas exchange, downstream advection, groundwater inputs of CO_2, and benthic respiration driven by turbulent mixing. These process-based predictions outperform statistical methods within the East River, and future work will test the accuracy of the stream network model when applied to other systems. The stream network model also provides direct estimates of the proportion of external and internal CO_2 contributions. The model suggests that hyporheic exchange needs to be modeled accurately as it represents a significant portion of stream CO_2 contributing 47% in the East River. Finally, through the direct comparison of existing statistical methods to the stream network model and sample data, we found that statistical upscaling of pCO_2 can cause a significant overestimation of CO_2 fluxes within the East River. Therefore, it is paramount that process-based models be applied at regional and global scales to accurately constrain the river and stream CO_2 emissions.

Acknowledgments and Data

We thank Jennifer Reithel, Ian Billick, and the Rocky Mountain Biological Laboratory staff for field and logistical support. We also thank Kate Maher, Corey Lawrence, David Boutt, and the Hydroseminar group at UMass Geosciences for useful conversations related to this paper. All data and code used in this work are available in the Supplemental Information for reviewers to access; further, the dataset will be available by the time of publication in the ESS-DIVE Database for public access, where it is currently under review.

References

Allen, G. H., & Pavelsky, T. M. (2018). Global extent of rivers and streams. *Science*, *361*(6402), 585–588. https://doi.org/10.1126/science.aat0636

Battaglin, W., Hay, L., & Markstrom, S. (2011). Simulating the potential effects of climate change in two Colorado basins and at two Colorado ski areas. *Earth Interactions*, *15*(22), 1–23. https://doi.org/10.1175/2011EI373.1

Bencala, K. E., & Walters, R. A. (1983). Simulation of solute transport in a mountain pool-and-riffle stream: A transient storage model. *Water Resources Research*, *19*(3), 718–724. https://doi.org/10.1029/WR019i003p00718

Borges, A. V., Darchambeau, F., Teodoru, C. R., Marwick, T. R., Tamooh, F., Geeraert, N., et al. (2015). Globally significant greenhouse-gas emissions from African inland waters. *Nature Geoscience*, *8*(8), 637–642. https://doi.org/10.1038/ngeo2486

Breugem, W., Boersma, B., & Uittenbogaard, R. (2006). The influence of wall permeability on turbulent channel flow. *J. Fluid Mech*, *562*, 35–72. https://doi.org/10.1017/S0022112006000887

Buffam, I., Laudon, H., Bishop, K., Öquist, M., & Wallin, M. (2010). Temporal and spatial variability of dissolved inorganic carbon in a boreal stream network: Concentrations and downstream fluxes. *Journal of Geophysical Research: Biogeosciences*, *115*(G2). https://doi.org/10.1029/2009jg001100

Butman, D., & Raymond, P. A. (2011). Significant efflux of carbon dioxide from streams and rivers in the United States. *Nature Geoscience*, *4*(10), 839–842. https://doi.org/10.1038/ngeo1294

Carroll, R., & Williams, K. (2019). Discharge data collected within the East River for the Lawrence Berkeley National Laboratory Watershed Function Science Focus Area (water years 2015-present). Retrieved from http://dx.doi.org/10.21952/WTR/1495380

Carroll, R. W. H., Bearup, L. A., Brown, W., Dong, W., Bill, M., & Willlams, K. H. (2018). Factors controlling seasonal groundwater and solute flux from snow-dominated basins. *Hydrological Processes*, *32*(14), 2187–2202. https://doi.org/10.1002/hyp.13151

Cole, J. J., Prairie, Y. T., Caraco, N. F., McDowell, W. H., Tranvik, L. J., Striegl, R. G., et al. (2007). Plumbing the global carbon cycle: Integrating inland waters into the terrestrial carbon budget. *Ecosystems*, *10*, 171–184. https://doi.org/10.1007/s10021-006-9013-8

Drake, T. W., Raymond, P. A., & Spencer, R. G. M. (2018). Terrestrial carbon inputs to inland waters: A current synthesis of estimates and uncertainty. *Limnology and Oceanography Letters*, *3*(3), 132–142. https://doi.org/10.1002/lol2.10055

Duvert, C., Butman, D. E., Marx, A., Ribolzi, O., & Hutley, L. B. (2018). CO2 evasion along streams driven by groundwater inputs and geomorphic controls. *Nature Geoscience*, *11*(11), 813–818. https://doi.org/10.1038/s41561-018-0245-y

Gaskill, D. L., Godwin, L. H., & Mutschler, F. E. (1967). *Geologic map of the Oh-Be-Joyful quadrangle, Gunnison County, Colorado*. *Geologic Quadrangle*. Washington, D. C. https://doi.org/10.3133/gq578

Gaskill, D. L., Mutschler, F. E., Kramer, J. H., Thomas, J. A., & Zahony, S. G. (1991). *Geologic Map of the Gothic quadrangle, Gunnison County, Colorado*. Washington, D. C.

Gomez-Velez, J. D., & Harvey, J. W. (2014). A hydrogeomorphic river network model predicts where and why hyporheic exchange is important in large basins. *Geophysical Research Letters*, *41*(18), 6403–6412. https://doi.org/10.1002/2014GL061099

Gomez-Velez, J. D., Harvey, J. W., Cardenas, M. B., & Kiel, B. (2015). Denitrification in the Mississippi River network controlled by flow through river bedforms. *Nature Geoscience*, *8*(12), 941–945. https://doi.org/10.1038/ngeo2567

Grant, S. B., Azizian, M., Cook, P., Boano, F., & Rippy, M. A. (2018). Factoring stream turbulence into global assessments of nitrogen pollution. *Science*, *359*(6381), 1266–1269. https://doi.org/10.1126/science.aap8074

Hartmann, J., Lauerwald, R., & Moosdorf, N. (2014). A Brief Overview of the GLObal RIver Chemistry Database, GLORICH. Procedia Earth and Planetary Science, 10, 23–27. https://doi.org/10.1016/j.proeps.2014.08.005

Harvey, J., Gomez-Velez, J., Schmadel, N., Scott, D., Boyer, E., Alexander, R., et al. (2019). How Hydrologic Connectivity Regulates Water Quality in River Corridors. *JAWRA Journal of the American Water Resources Association*, *55*(2), 369–381. https://doi.org/10.1111/1752-1688.12691

Hengl, T., De Jesus, J. M., Heuvelink, G. B. M., Gonzalez, M. R., Kilibarda, M., Blagotić, A., et al. (2017). SoilGrids250m: Global gridded soil information based on machine learning. *PLoS ONE*, *12*(2), e0169748–e0169748. https://doi.org/10.1371/journal.pone.0169748

Hope, D., Palmer, S. M., Billett, M. F., & Dawson, J. J. C. (2004). Variations in dissolved CO2 and CH4 in a first-order stream and catchment: An investigation of soil-stream linkages. *Hydrological Processes*, *18*(17), 3255–3275. https://doi.org/10.1002/hyp.5657

Horgby, Å., Boix Canadell, M., Ulseth, A. J., Vennemann, T. W., & Battin, T. J. (2019). High-Resolution Spatial Sampling Identifies Groundwater as Driver of CO2 Dynamics in an Alpine Stream Network. *Journal of Geophysical Research: Biogeosciences*, *124*(7), 1961–1976. https://doi.org/10.1029/2019JG005047

Horgby, Å., Segatto, P. L., Bertuzzo, E., Lauerwald, R., Lehner, B., Ulseth, A. J., et al. (2019). Unexpected large evasion fluxes of carbon dioxide from turbulent streams draining the world's mountains. *Nature Communications*, *10*(1), 4888. https://doi.org/10.1038/s41467-019-12905-z

Hotchkiss, E. R., Hall Jr, R. O., Sponseller, R. A., Butman, D., Klaminder, J., Laudon, H., et al. (2015). Sources of and processes controlling CO 2 emissions change with the size of streams and rivers. *Nature Geoscience*, *8*(9), 696–699. https://doi.org/10.1038/ngeo2507

Hubbard, S. S., Williams, K. H., Agarwal, D., Banfield, J., Beller, H., Bouskill, N., et al. (2018). The East River, Colorado, Watershed: A Mountainous Community Testbed for Improving Predictive Understanding of Multiscale Hydrological-Biogeochemical Dynamics. *Vadose Zone Journal*, *17*(1), 180061. https://doi.org/10.2136/vzj2018.03.0061

Jähne, B., Heinz, G., & Dietrich, W. (1987). Measurement of the diffusion coefficients of sparingly soluble gases in water. *Journal of Geophysical Research*, *92*(C10), 10767. https://doi.org/10.1029/JC092iC10p10767

Johnson, M.S., Lehmann, J., Riha, S.J., Krusche, A.V., Richey, J.E., Ometto, J.P.H.B., Couto, E.G. (2009) CO_2 efflux from Amazonian headwater streams represents a significant fate for deep soil respiration. Geophysical Research Letters 35(17), GL034619.

Lauerwald, R., Laruelle, G. G., Hartmann, J., Ciais, P., & Regnier, P. A. G. (2015). Spatial patterns in CO 2 evasion from the global river network. *Global Biogeochemical Cycles*, *29*(5), 534–554. https://doi.org/10.1002/2014GB004941

Lupon, A., Denfield, B.A., Laudon, H., Leach, J., Karlsson, J., Sponseller, R.A. (2019) Groundwater inflows control patterns and sources of greenhouse gas emissions from streams. Limnology and Oceanography 9999, 1-13.

Markstrom, S. L., & Hay, L. E. (2009). Integrated Watershed Scale Response to Climate Change for Selected Basins Across the United States Author (s): Steven L . Markstrom and Lauren E . Hay Source : Water Resources IMPACT , Vol . 11 , No . 2 , Managing Water Resources Development in a Changi, *11*(2), 8–10.

Marx, A., Dusek, J., Jankovec, J., Sanda, M., Vogel, T., van Geldern, R., et al. (2017). A review of CO 2 and associated carbon dynamics in headwater streams: A global perspective. *Reviews of Geophysics*, *55*(2), 560–585. https://doi.org/10.1002/2016RG000547

Marzadri, A., Dee, M. M., Tonina, D., Bellin, A., & Tank, J. L. (2017). Role of surface and subsurface processes in scaling N2O emissions along riverine networks. *Proceedings of the National Academy of Sciences of the United States of America*, *114*(17), 4330–4335. https://doi.org/10.1073/pnas.1617454114

Morrison, S. J., Goodknight, C. S., Tigar, A. D., Bush, R. P., & Gil, A. (2012). Naturally Occurring Contamination in the Mancos Shale. https://doi.org/10.1021/es203211z

NASA. (2019). MODIS Gross Primary Production (GPP)/Net Primary Production (NPP). Retrieved from https://modis.gsfc.nasa.gov/data/dataprod/mod17.php

Nelson, A. R., Sawyer, A. H., Gabor, R. S., Saup, C. M., Bryant, S. R., Harris, K. D., et al. (2019). Heterogeneity in Hyporheic Flow, Pore Water Chemistry, and Microbial Community Composition in an Alpine Streambed. *Journal of Geophysical Research: Biogeosciences*, *124*(11), 3465–3478. https://doi.org/10.1029/2019JG005226

Newcomer, M., & Rogers, D. B. (2020). Gap-filled meteorological data (2011-2020) and modeled potential evapotranspiration data from the KCOMTCRE2 WeatherUnderground weather station, from the East River Watershed, Colorado. Watershed Function SFA. https://doi.org/10.15485/1734790

PRISM. (2013). Parameter-elevation Regressions on Independent Slopes Model. Retrieved May 28, 2020, from http://www.prism.oregonstate.edu/normals/

R Core Team. (2020). R: A language and environment for statistical computing. Vienna, Austria: R Foundation for Statistical Computing. Retrieved from https://www.r-project.org/

Rasilo, T., Hutchins, R. H. S., Ruiz-González, C., & del Giorgio, P. A. (2017). Transport and transformation of soil-derived CO2, CH4and DOC sustain CO2supersaturation in small boreal streams. *Science of the Total Environment*, *579*, 902–912. https://doi.org/10.1016/j.scitotenv.2016.10.187

Raymond, P. A., Zappa, C. J., Butman, D., Bott, T. L., Potter, J., Mulholland, P., et al. (2012). Scaling the gas transfer velocity and hydraulic geometry in streams and small rivers. *Limnology and Oceanography: Fluids and Environments*, *2*(2012), 41–53. https://doi.org/10.1215/21573689-1597669

Raymond, P. A., Hartmann, J., Lauerwald, R., Sobek, S., Mcdonald, C., Hoover, M., et al. (2013). Global carbon dioxide emissions from inland waters. *Nature*, *503*(7476), 355–359. https://doi.org/10.1038/nature12760

Rocher-Ros, G., Sponseller, R. A., Lidberg, W., Mörth, C., & Giesler, R. (2019). Landscape process domains drive patterns of CO 2 evasion from river networks. *Limnology and Oceanography Letters*, *4*, 87–95. https://doi.org/10.1002/lol2.10108

Sawakuchi, H. O., Neu, V., Ward, N. D., Barros, M. de L. C., Valerio, A. M., Gagne-Maynard, W., et al. (2017). Carbon Dioxide Emissions along the Lower Amazon River. *Frontiers in Marine Science*, *4*, 76. https://doi.org/10.3389/fmars.2017.00076

Steefel, C. I., Appelo, C. A. J., Arora, B., Jacques, D., Kalbacher, T., Kolditz, O., et al. (2015). Reactive transport codes for subsurface environmental simulation. *Computational Geosciences*, *19*(3), 445–478. https://doi.org/10.1007/s10596-014-9443-x

Steefel, Carl I., DePaolo, D. J., & Lichtner, P. C. (2005). Reactive transport modeling: An essential tool and a new research approach for the Earth sciences. *Earth and Planetary Science Letters*, *240*(3–4), 539–558. https://doi.org/10.1016/j.epsl.2005.09.017

U.S. Geological Survey. (2019). National Hydrography Dataset Plus High Resolution. Retrieved from https://www.usgs.gov/core-science-systems/ngp/national-hydrography/nhdplus-high-resolution

Ulseth, A. J., Hall, R. O., Boix Canadell, M., Madinger, H. L., Niayifar, A., & Battin, T. J. (2019). Distinct air–water gas exchange regimes in low- and high-energy streams. *Nature Geoscience*, *12*(4), 259–263. https://doi.org/10.1038/s41561-019-0324-8

Wanninkhof, R. (1992). Relationship between wind speed and gas exchange over the ocean. *Journal of Geophysical Research*, *97*(C5), 7373–7382. https://doi.org/10.1029/92JC00188

Ward, N. D., Keil, R. G., Medeiros, P. M., Brito, D. C., Cunha, A. C., Dittmar, T., et al. (2013). Degradation of terrestrially derived macromolecules in the Amazon River. *Nature Geoscience*, *6*(7), 530–533. https://doi.org/10.1038/ngeo1817

Winnick, M. J., Carroll, R. W. H., Williams, K. H., Maxwell, R. M., Dong, W., & Maher, K. (2017). Snowmelt controls on concentration-discharge relationships and the balance of oxidative and acid-base weathering fluxes in an alpine catchment, East River, Colorado. *Water Resources Research*, *53*(3), 2507–2523. https://doi.org/10.1002/2016WR019724

Winnick, M. J., Lawrence, C. R., McCormick, M., Druhan, J. L., & Maher, K. (2020). Soil Respiration Response to Rainfall Modulated by Plant Phenology in a Montane Meadow, East River, Colorado, USA. *Journal of Geophysical Research: Biogeosciences*, *125*(10). https://doi.org/10.1029/2020JG005924